J Mater Sci (2008) 43:440–449
DOI 10.1007/s10853-007-1982-2

5TH BRAZILIAN MRS MEETING

Rh/CeO_2 catalyst preparation and characterization for hydrogen production from ethanol partial oxidation

L. O. O. Costa · S. M. R. Vasconcelos · A. L. Pinto · A. M. Silva · L. V. Mattos · F. B. Noronha · L. E. P. Borges

Received: 29 December 2006 / Accepted: 6 July 2007 / Published online: 27 September 2007

Abstract Hydrogen production for fuel cells from ethanol partial oxidation was evaluated on 1% Rh/CeO_2 catalyst. Transmission Electron Microscopy (TEM) and Scanning Electron Microscopy (SEM) were used to analyze carbon formation and the possible sintering of the metallic phase. X-ray fluorescence (XRF), nitrogen adsorption, and temperature-programmed reduction (TPR) were also used for catalyst characterization. Two groups of rhodium particles of different sizes were observed. By SEM/EDS analysis, no residual chloride was identified. TEM made it possible to identify the presence of rhodium in small clusters. On the other hand, products distribution was affected by reaction temperature. At 473 K, only traces of acetaldehyde were detected for the Rh/CeO_2 catalyst. In the reaction conditions, no deactivation of the catalyst due to carbon deposition or sintering of the metal was observed. Overall, our results show that the performance of Rh/CeO_2 catalyst points to promising applications in terms of H_2 production for fuel cells technology by ethanol partial oxidation.

L. O. O. Costa · L. E. P. Borges
Instituto Militar de Engenharia, Seção de Química, Pç General Tibúrcio 80, Rio de Janeiro CEP 22290-270 RJ, Brazil

L. O. O. Costa · A. M. Silva · L. V. Mattos · F. B. Noronha (✉)
Instituto Nacional de Tecnologia, Laboratório de Catálise, Avenida Venezuela, 82, sl. 518, Rio de Janeiro CEP 20081-312 RJ, Brazil
e-mail: fabiobel@int.gov.br

S. M. R. Vasconcelos
NUCAT/PEQ/COPPE—Universidade Federal do Rio de Janeiro, Centro de Tecnologia, Bl. G, sala 128, Rio de Janeiro CEP 21945-970 RJ, Brazil

A. L. Pinto
Instituto Militar de Engenharia, Seção de Engenharia Mecanica-Materiais, Pç General Tibúrcio 80, Rio de Janeiro CEP 22290-270 RJ, Brazil

Introduction

It is well known that the use of fossil fuels, such as petroleum and coal, is limited, non-renewable and brings environmental problems. Therefore, alternative resources have been developed to meet the world's growing demand for energy [1]. Hydrogen is a promising alternative to those fuels and will certainly be widely used in a decade or so. It is an excellent energy carrier when used directly in fuel internal combustion engines or, indirectly, to supply electricity using fuel cells. Energy production via fuel cells is not subject to thermodynamic limitations imposed by the Carnot cycle and, thus, presents higher efficiency when compared to conventional combustion engines. Fuel cells may present electric efficiencies around 40–50%, and they can reach 80–85% rates when heat is used to advantage [2, 3].

Nowadays, hydrogen production technology is well established for large units (10,000–100,000 Nm^3/h or larger), and it is based on hydrocarbon steam reforming. However, the installed hydrogen production and distribution infrastructure is insufficient to support its widespread use in a hydrogen-based economy. In the absence of a hydrogen infrastructure in the early stage of the transition to a hydrogen-based economy, hydrogen should be produced locally at fuel stations, which poses additional challenges. The development of small fuel processors is critical for distributed generation systems or facilities as well as for vehicles [4].

The major drawback to the wider use of hydrogen as an energy source is the inherent difficulty regarding storage and distribution of this gas. Methanol, ethanol, and natural gas are the most important candidates for an efficient production of hydrogen for stationary power plants and vehicles. A solution to these problems is the on-board hydrogen generation from a suitable high energy density liquid fuel. Ethanol presents advantages when compared to the other two candidates, as it can be easily extracted from renewable sources [1] (such as sugar cane), it is less toxic than methanol and, in the Brazilian case, the infrastructure for ethanol production and distribution is already organized through a large distribution network. Hydrogen production from ethanol can be achieved by steam reforming, partial oxidation and autothermal reforming. Currently, research has mostly focused on the steam reforming technology. However, this reaction is highly endothermic and high steam/C ratios are required in order to avoid carbon formation. On the other hand, there are a few studies dealing with partial oxidation of ethanol [5–9]. This process presents some advantages over steam reforming such as fast start up and short response time. Besides the reactor for partial oxidation is smaller than that used for steam reforming, once no additional heat is needed for the reaction, which is exothermic [5].

Ethanol reactions occur by a complex mechanism, including multiple reactions [10], and the control of selectivity of such reactions is crucial because hydrocarbons and oxygenates can be produced. Products distribution and catalyst stability are correlated to the nature of the metal (M) and/or the support [11]. Indeed, Mattos and Noronha [5] have shown that product distribution from ethanol partial oxidation is affected by the nature of the metal (Pd, Pt and Co) of ceria-supported catalysts. According to their results, acetaldehyde was the only product detected over Co/CeO_2 catalyst, while methane was also produced on Pt/CeO_2 and Pd/CeO_2 [5]. A reaction mechanism was proposed to explain the previously obtained results. Likewise, ethanol partial oxidation pathway over Ru/Y_2O_3 differs from that over Pd/Y_2O_3 [7]. Moreover, the route for Hydrogen production on Rh catalysts occurs by a distinct mechanism through a cyclic intermediate formation, indicating that ethanol adsorption is greatly affected by the metal characteristics [12]. Additionally, Rh/CeO_2 (Rh alone or in presence of a second metal, such as Pd or Pt) has shown interesting activity for ethanol decomposition in presence of oxygen [13–14]. This activity is attributed to Rh capacity to break carbon–carbon bonds, a required step for an efficient total decomposition of ethanol [15]. On the other hand, in some studies, Rh sintering was observed for high temperatures in methane partial oxidation and ethanol autothermal reforming reactions, which is attributed to its high activity and selectivity [12–16]. The support properties can affect catalytic performance drastically in the steam reforming of methanol and ethanol [16]. However, there are a few works dealing with the effect of the support on ethanol partial oxidation [6–8]. Our research has shown that products distribution obtained over these catalysts has been associated to their redox and acid properties.

Supports with redox properties exhibit a distinct characteristic because they are partially reducible under reduction conditions, which have been currently related to Strong Metal Support Interaction (SMSI) effect. The term SMSI was first introduced in 1978 to describe the behavior of titanium oxide over the chemisorption properties of group VIII metals when reduced at high temperatures (>573 K) [17]. Support reduction stems from non-stoichiometric oxides (TiO_x, CeO_x) that migrate over the metal surface creating special sites at the metal support interface. These sites are formed by at least one atom at a metal adjacent to a defect site on the support [18].

Concerning partially reducible oxides, CeO_2 has been commonly reported as a catalyst support in a wide variety of reactions, including oxidation or partial oxidation of hydrocarbons (e.g., automotive catalysts). Ceria-supported catalysts have good resistance to coke formation. This resistance can be associated not only with SMSI but also with high oxygen mobility in the ceria lattice (redox property) due to a fluorite structure—a relatively open one, allowing easy oxygen diffusion. Hence, this ability confers on ceria very interesting features for catalytic applications (e.g., CO direct oxidation and water gas shift) [19].

Nevertheless, hydrogen production from ethanol has some disadvantages such as catalytic deactivation by carbon formation [14]. The route of carbon formation will influence its morphology. The most common types of carbon deposition are filamentous carbon and pyrolitic carbon [20]. Carbon formation mechanisms found for Rh/Al_2O_3 catalysts were previously reported by Cavallaro et al. [14]. Those authors found a small amount of carbon whiskers, but no encapsulating shell or pyrolitic carbon was observed.

The aim of this work is to study the Rh/CeO_2 catalytic behavior in the partial oxidation of ethanol. A detailed investigation into the distribution and morphology of the active phase (before and after catalytic tests) is herein presented. This information should contribute to the design of more efficient catalysts for hydrogen production for fuel cells technology by ethanol partial oxidation.

Experimental

CeO_2 support was prepared by calcination of cerium (IV) ammonium nitrate (Sigma) at 1073 K for 1 h in a muffle furnace. The catalyst was prepared by incipient wetness

impregnation of the support with an aqueous solution containing $RhCl_3.H_2O$ (Sigma). After impregnation, the samples were dried at 393 K and calcined under air (30 cm^3/min) at 673 K for 2 h.

The chemical composition of the sample was determined by X-Ray Fluorescence on a Rigaku RIX3100 equipment. The surface areas of the catalyst and the support were measured by nitrogen adsorption at liquid nitrogen temperature using a Micromeritics ASAP 2000 analyzer. X-Ray diffratogram were collected using a Rigaku-Miniflex equipment with a Cu radiation (Kα-1.5406 Å) at a 2θ interval of 5–90°, with a step size of 0.02° per minute.

TPR experiments were conducted by using 300 mg of catalyst in a fixed-bed quartz reactor under 1.5% H_2 in argon (30 mL/min) with a heating rate of 10 K/min from 473 K to 1273 K. Hydrogen consumption rate was monitored by a thermal conductivity detector (TCD).

As for scanning electron microscopy (SEM) and transmission electron microscopy (TEM) analyses, the sample was first reduced with H_2 at 30 mL/min raising the temperature at a 10 K/min rate, from 298 K to 773 K. In sequence, the sample was passivated with 2% O_2/He at 77 K for 30 min, and at 298 K for 1 h [21]. Catalyst morphology was characterized with a JEOL JSM-6460 LV scanning electron microscope. It was equipped with a secondary electron analysis detector. The microscope was also equipped with a Thermo/Noran (System Six 200) energy dispersive spectrometer (EDS).

Transmission electron microscopy analyses were carried out in a JEOL 2010 equipment operated in imaging mode. The microscope was equipped with a Thermo/Noran EDS. For the fresh catalyst, the sample was dispersed in acetone, deposited on a carbon-coated grid and, then, the solvent was evaporated. For the residue, the sample was ground and placed in an oven until fine particles were obtained. A sampling of the powder was taken by using a syringe and deposited on a carbon-coated grid. By using TEM, it was possible to analyze particle diameter, dispersion, possible sinterization and coke formation. Particle diameters were measured using Axion Vision 4.0 software.

Ethanol partial oxidation tests were performed in a fixed-bed reactor at atmospheric pressure. In order to avoid hot spots formation and temperature gradients, the catalyst samples (160 mg) were diluted with inert SiC (catalyst/SiC ratio = 1/3) to form a small catalytic bed (<5 mm in height). The temperature of the catalyst bed was measured through a thermocouple inserted into a small cavity at the reactor wall. Prior to the reaction, the samples were reduced under H_2 at 733 K for 1 h. The reactants were fed to the reactor by bubbling air (30 cm^3/min) and N_2 (30 cm^3/min) through a saturator containing ethanol at 313 K in order to obtain the desired ethanol/O_2 molar ratio (2/1). The reaction was carried out at different temperatures. The exit gases were analyzed using a gas chromatograph (VARIAN, CP 3800) equipped with two columns (molecular sieve and parabound Q/CP 7424-Select Permanent Gases/CO_2) coupled in parallel, flame ionization and thermal conductivity detectors connected in series.

Carbon formation over the catalyst was analyzed by thermogravimetric analysis (TGA) using a TA instruments equipment (TGA 2050). The sample was heated under air from room temperature to 1273 K at a heating rate of 5 K/min.

Results and discussion

Chemical properties

BET measurements indicated that the specific surface area of the catalyst was 11.7 m^2/g, whereas the specific surface area of the support was 9.9 m^2/g. Such values are commonly expected for ceria and ceria supported catalysts.

Fluorescence analysis indicated 1.1% of metallic rhodium in the catalyst.

The metal oxidation state over CeO was investigated by XRD analysis. XRD patterns of CeO_2 support, as well as 1% Rh/CeO_2 catalyst, exhibited CeO_2 phase diffraction lines. Apart from these, no lines related to Rh were found (Fig. 1) [22]. Although metal loading was rather low, the absence of diffraction lines of Rh_2O_3 could be associated with a high dispersion degree of the supported phase.

TPR behavior

The surface and bulk reducibility of Rh/CeO_2 catalyst were studied by TPR. The TPR profile is shown in Fig. 2. The

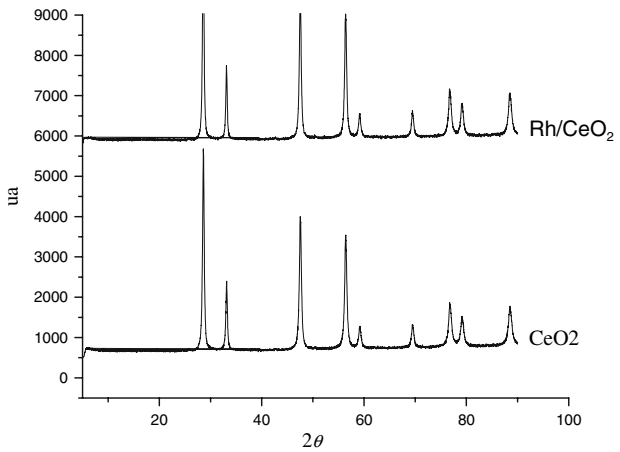

Fig. 1 XRD patterns of CeO_2 support and 1% Rh/CeO_2 catalyst reduced in hydrogen at 673 K

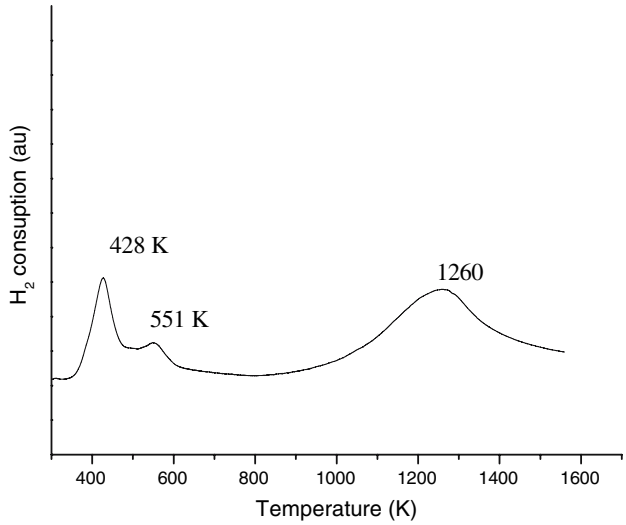

Fig. 2 TPR profile of the 1% Rh/CeO_2 catalyst

presence of two peaks could indicate that the Rh ions would be present in two distinct electronic states. However, previous Diffuse Reflectance Spectroscopy (DRS) results (Fig. 3) showed just one absorption region [23], which is in accordance with Mendes and Schmal's studies [24] regarding bulk rhodium oxide. Indeed, different metal-support interactions would explain the presence of the two TPR peaks [10]. TPR analysis identified the presence of Rh_2O_3, which was reduced to metallic rhodium at temperatures lower than 573 K.

The low temperature peak (428 K) is attributed to particles with weak interaction with the support, while the second peak (551 K) is attributed to the reduction of a bulk-like crystalline Rh_2O_3 on the surface. The peak at c.a 1260 K is assigned to the bulk reduction of the support (Ce^{+4} to Ce^{+x}, $x < 4$). The reduction reactions are as folllows (1 and 2):

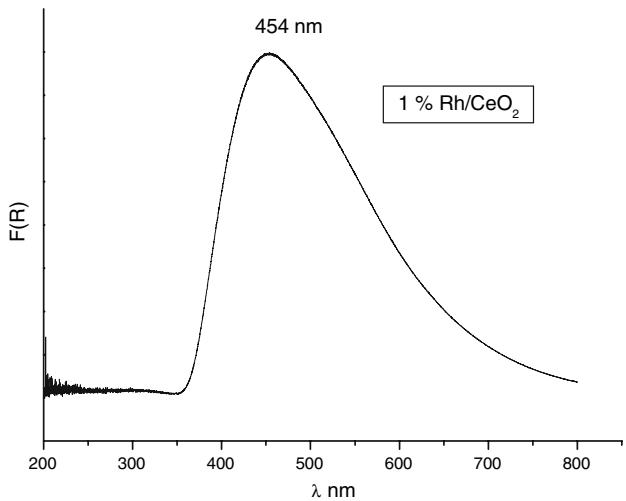

Fig. 3 DRS spectrum of 1% rhodium catalyst

$$Rh_2O_3 + 3H_2 \rightarrow 2Rh + 3H_2O \ (428\text{--}551\ K) \quad (1)$$

$$2CeO_2 + H_2 \rightarrow Ce_2O_3 + H_2O \ (1260\ K) \quad (2)$$

SEM and TEM of fresh catalyst

Figure 4 presents the secondary electrons image obtained by SEM analysis of fresh Rh/CeO_2 reduced at 773 K. Rich regions of Rh and CeO_2 were identified by energy dispersive spectroscopy (EDS).

The chlorine ions originated from the metal salt precursor can be strongly retained by the support [14] and can influence the catalyst properties. EDS analysis indicates no residual chlorine after calcination. This result is in agreement with the BET results, indicating that no chlorine was

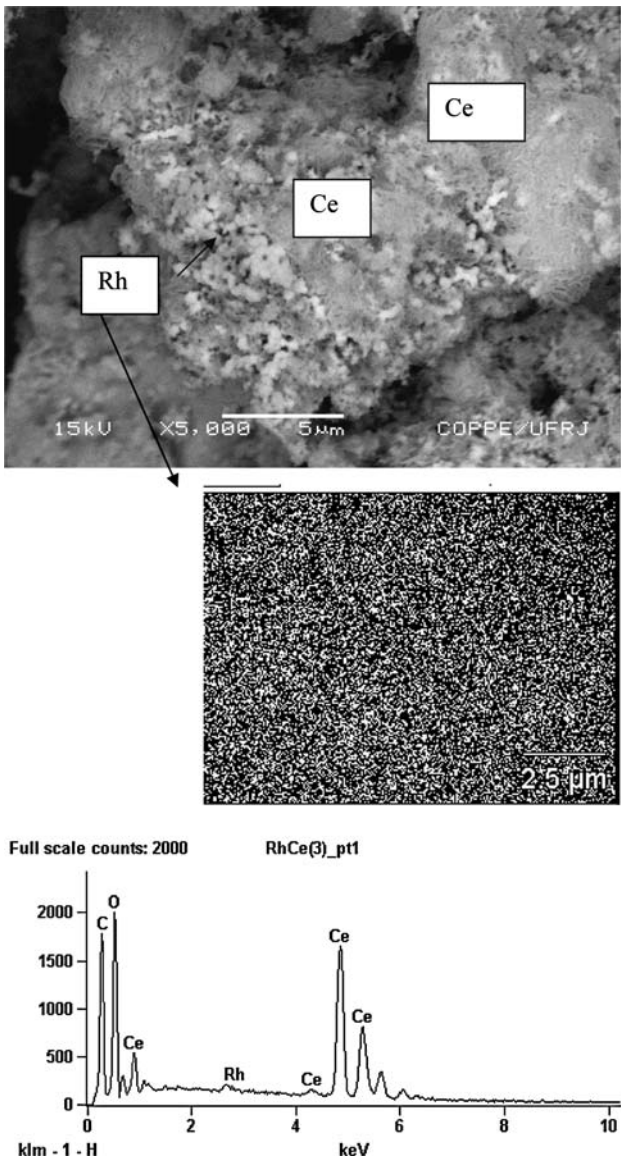

Fig. 4 SEM image with EDS Mapping

incorporated into the support and that the calcination treatment was effective. EDS mapping indicated that rhodium was uniformly distributed over the support.

Figures 5, 6, 7 present images of bright field obtained by TEM of 1% Rh/CeO_2 sample reduced at 773 K. The nature of the individual Rh metallic particles was confirmed by EDS. The determination of Rh/CeO_2 in crystallite size in catalyst with TEM was facilitated by differences observed in the contrast between dark Rh particles and white ceria carrier due to the difference in atomic number.

In Fig. 6, Rhodium particles sizes ranged between 0.4 nm and 7.9 nm. It was also observed that, besides the spheroidal shape, a kind of hexagonal shape can also be observed, in agreement with similar results that have been reported by Benal et al. [25].

The TEM micrography presented in Fig. 7 suggests the existence of two density levels that can be distinguished within some of the darker particles. This suggests the presence of three dimensional terraced particles [26]. Particles of individual ceria of 8–15 nm size were measured directly with Axion Vision software. Moiré fringes formed by the overlap of CeO_2 and Rh are clearly visible, and the presence of pores can be observed.

A particle size distribution histogram obtained from the TEM images of 1% Rh/CO_2 catalyst is shown in Fig. 8. Particle size ranging from 0.4 nm to 15 nm was found. An average particle size of 5.4 nm and a dispersion of 17% were calculated from these data.

The particles of rhodium were preferentially found in presence of aggregates on the surface of CeO_2. Rhodium aggregate diameters found in this work are in accordance

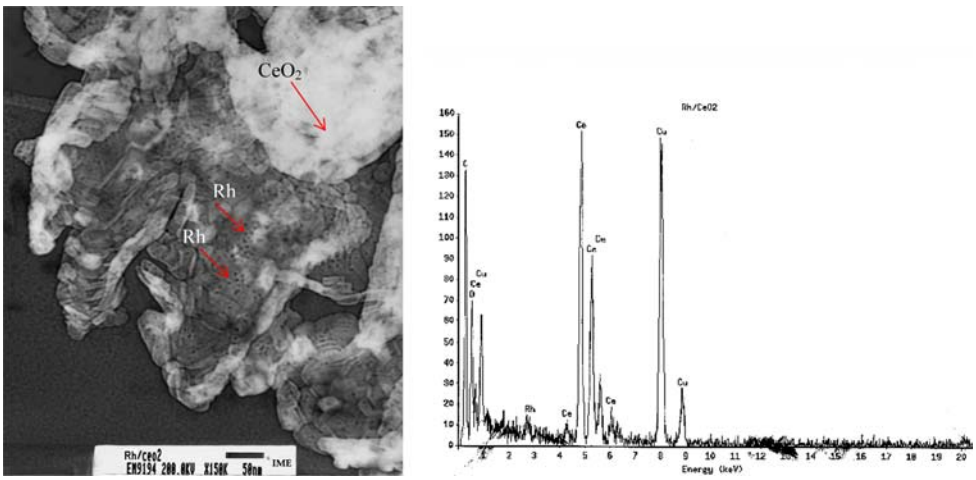

Fig. 5 TEM micrograph of Rh/CeO_2 with 150× magnification and EDS spectrum

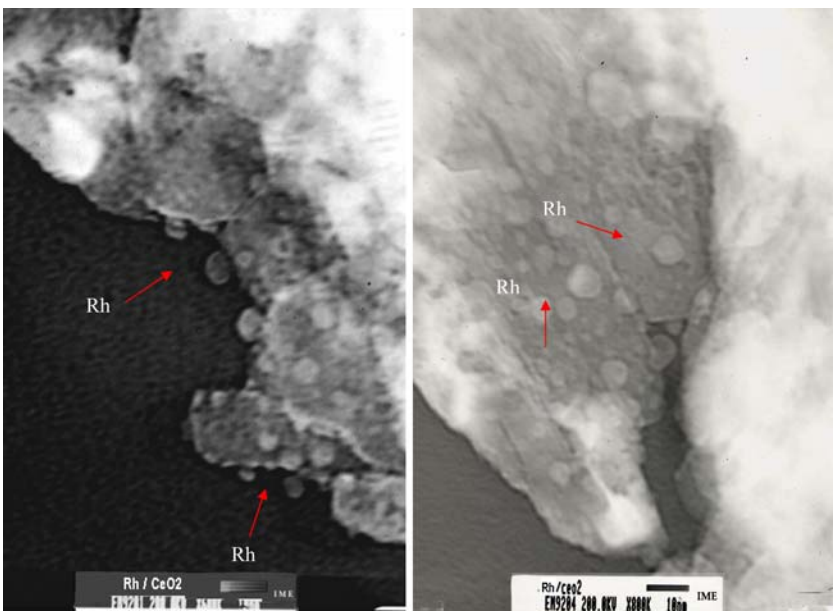

Fig. 6 TEM micrographs of Rh/CeO_2 with 600× and 800× magnification

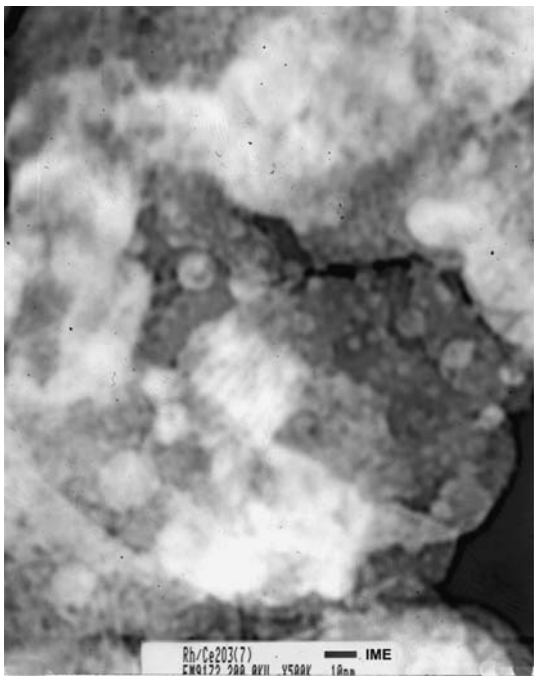

Fig. 7 TEM micrographs of Rh/CeO_2 with 500× magnification

with the rafts proposed by Graydon and Lagan [26]. According to these authors, rafts present diameters less than 2.0 nm for supported rhodium catalysts with contents at 0.64–1.94%.

Catalytic test—ethanol partial oxidation

The ethanol partial oxidation reaction was carried out in a wide range of temperatures (473–1073 K) using a stoichiometric ratio of O_2: ETOH (2:1). Ethanol conversion ($x_{ethanol}$) and product distribution obtained from the reaction over Rh/CeO_2 catalyst are presented in Fig. 9.

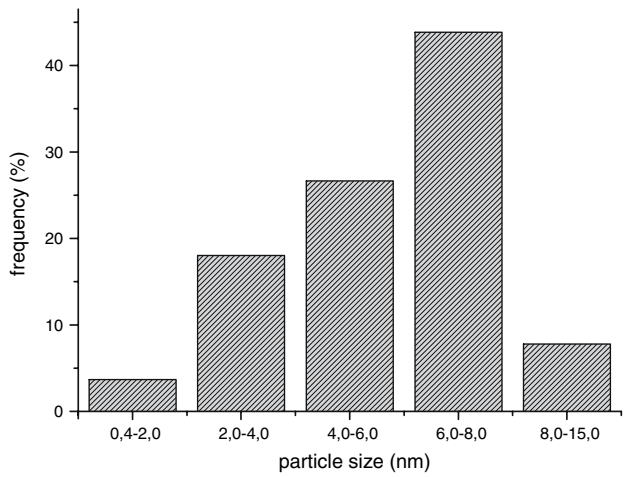

Fig. 8 Particle size distribution histogram of Rh/CeO_2

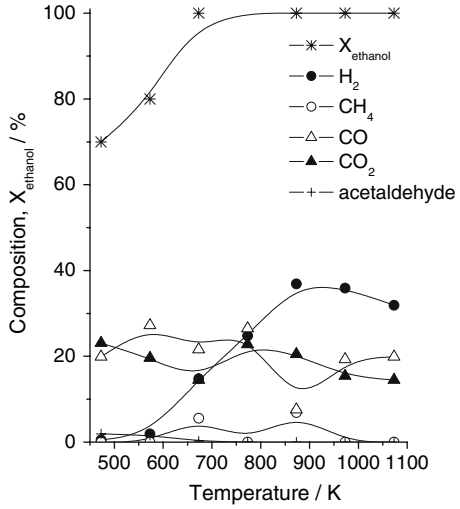

Fig. 9 Distribution of products and conversion of ethanol obtained for Rh/CeO_2 in ethanol partial oxidation in different temperatures

According to our results, the profiles of the products are strongly affected by reaction temperature.

The conversion of ethanol was complete at 650 K. It was observed that the reaction temperature increase led to an increase in hydrogen production; with a maximum at 873 K. Low methane formation was observed at all temperatures.

The catalyst presented significant formation of CO even at 473 K. The selectivity to CO_2 was essentially constant up to 873 K; in temperatures higher than 873 K, CO_2 formation was reduced. The formation of CO and CO_2 would be due to dissociation of intermediary cyclic compounds that were detected by HREELS (High Resolution Electron Energy Loss) and IR (Infrared) experiments performed by Jones et al. [27]. The reduction of water formation was observed for temperatures above 400 K. Acetaldehyde formation was not observed for all tests.

These results are consistent with those from the work of Sheng et al. [28], who worked with a $Rh–Pt/CeO_2$ catalyst. Increasing the reaction temperatures from 473 K to 673 K, the authors observed a decrease of acetaldehyde production and an increase of methane formation.

Although rhodium catalyst follows the dissociation of the cyclic compound route preferentially, it is not excluded that some fraction of ethoxy species follow the reaction route proposed by Mattos and Noronha [1, 5, 6] for ethanol partial oxidation over Pd/CeO_2 and Pt/CeO_2. In this route, the ethoxy species can be dehydrogenated, producing acetaldehyde, which readily reacts with oxygen and produces acetate species. The results obtained in this work could be explained by the reaction mechanism proposed by Silva et al. [9] (Fig. 10).

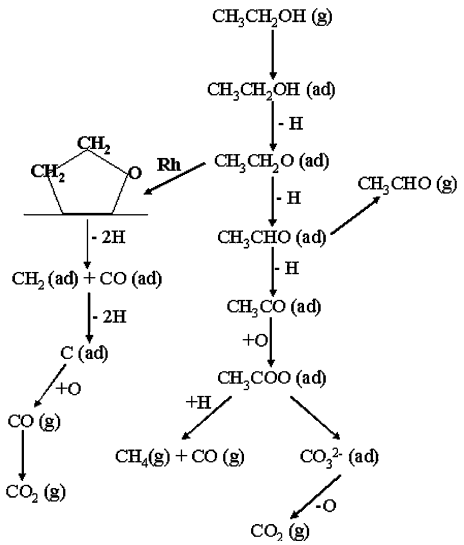

Fig. 10 Mechanism proposed for the reaction of ethanol partial oxidation in the metals surface [7]

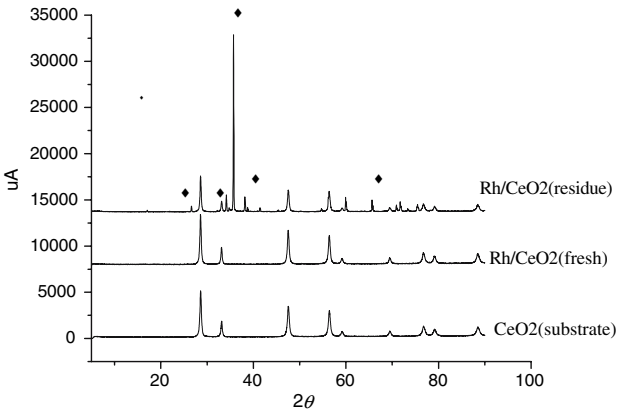

Fig. 12 XRD patterns of the samples of the fresh catalyst, residue and substrate. (◆) SiC. Peaks not marked correspond to CeO_2

TGA

To verify the possible formation of carbon proposed by Silva et al. [9], Rh/CeO_2 catalyst used was submitted to thermogravimetric analysis (TGA) to assess the amount of carbon eventually formed. TGA and its derivative (DTG) profiles are presented in Fig. 11. Rh/CeO_2 did not exhibit mass loss. This result is in agreement with TEM micrographs of the catalyst, where no filamentous carbon or carbon whiskers were observed.

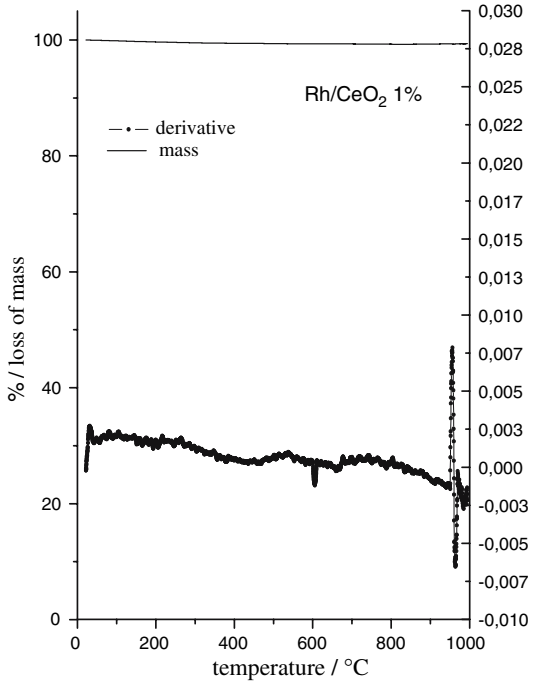

Fig. 11 Thermogravimetric analysis and first derivative (DTG) of the Rh/CeO_2 under air flow (30 mL/min) at heating rate 5 °C/min

These results can be explained considering the oxygen storage capacity of the ceria support. The high quantity of oxygen vacancies near the metallic particles allows an electronic transfer between metals ($Ce^{4+} \rightarrow Ce^{3+}$) with carbon removal from the metal surface and regeneration of the metal surface (auto cleaning mechanism of the catalytic surface [7]).

SEM and XRD after catalytic test

The fresh catalyst and residue were ground before SEM and XRD analyses so as to obtain uniformly distributed particles. In order to check the possible formation of a new metallic phase after reaction, XRD analysis of the residue was performed. Diffractograms (substrate, fresh catalyst and residue) were compared, and only diffraction lines corresponding to silicon, rhodium and ceria were identified (Fig. 12). The same reaction conditions were simulated before SEM analysis, and the fresh catalyst was diluted with silicon at a 3:1 ratio.

To develop SEM analysis, the powder material was coated with carbon, taking into account that the greater intensity band of Si is closer to the one of Au. Overall, SEM/EDS indicate (1400× image) irregular distribution of CeO_2 over silicon. EDS spectra do not reveal the presence of rhodium, which may indicate that the metal loading could be lower than EDS detection limit (around 1%). As a consequence, Rh was detected only by bulk analysis with a 10,000× magnification. (Figs. 13 and 14)

Silicon was added to the catalyst to avoid hot spot formation during reaction. However, as SEM analysis indicates, that distribution is not homogeneous, and the possibility of hot spot formation during reaction cannot be discarded.

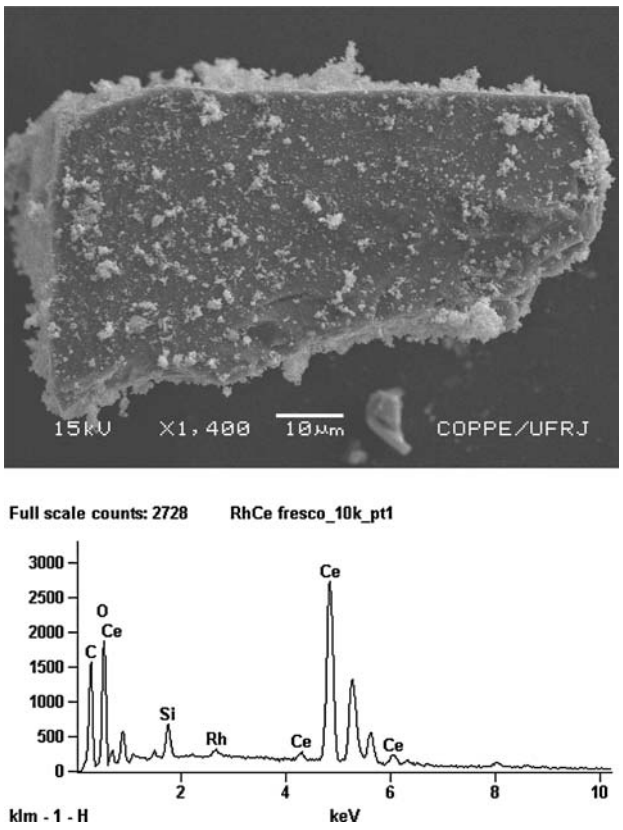

Fig. 13 Micrograph of fresh Rh/CeO_2 (dilluted with silicon and ground), and EDS bulk of fresh catalyst diluted with SiC with 10,000× magnification

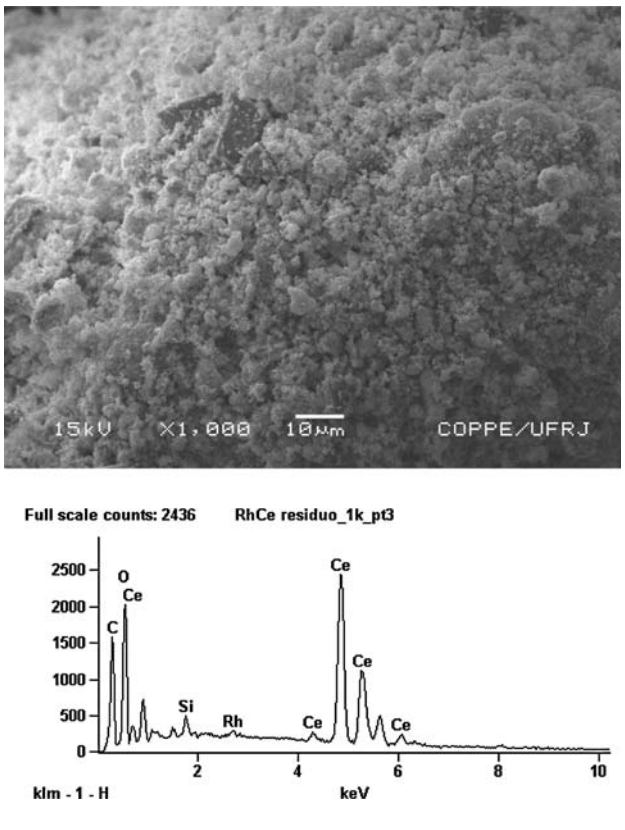

Fig. 14 SEM image (1,000× magnification) of Rh/CeO_2 residue (ground), and the correspondent EDS of the fresh catalyst diluted with SiC

TEM after catalytic test

TEM micrographs are shown in Fig. 15a–c, with 80,000×, 800,000× and 1 Mx.

Particle size distribution was evaluated from the TEM images (Fig. 15a–c) of the catalyst residue. A histogram was constructed and is displayed in Fig. 16. Particle size ranging from 0.94 nm to 6.6 nm from residue was determined. An average particle size of 5.1 nm and dipersion was 19%. Comparing both catalysts, fresh and residue, it is found that particle diameter was quite similar, indicating no sinterization.

As for TEM images, different phases may be noted, which are associated with the presence of silicon, ceria and rhodium, as observed by EDS analysis (not shown). After magnifying detail A of Fig. 15a up to 1M, it was found that Rh particles would be recovered by CeO_2. According to Wang and Ruckenstein's works [11], possible decoration of rhodium crystallite by a thin layer of support is suggested. That effect is attributed to SMSI (strong metal-support interaction), which can be either of a geometric or electronic nature, covering the metal crystallite by the reduced support. Electron Energy Loss Spectroscopy (EELS) will be conducted for a better understanding of these results [29].

Conclusion

Catalysts operating under the present reaction conditions have shown to be efficient for ethanol partial oxidation reaction, being highly active, selective, and stable. In this work, as temperature increased, acetaldehyde formation was suppressed, and H_2 formation increased.

Regarding metallic rhodium distribution over ceria, TEM analysis for the fresh catalyst revealed distinct metal particle diameters, which would be associated with the presence of rhodium clusters. According to TEM analysis of the fresh catalyst and residue, it was found that neither sintering nor coke formation occurred, which was confirmed by TGA analysis. Overall, our results show that the performance of Rh/CeO_2 catalyst points to promising applications in terms of H_2 production for fuel cell technology by ethanol partial oxidation.

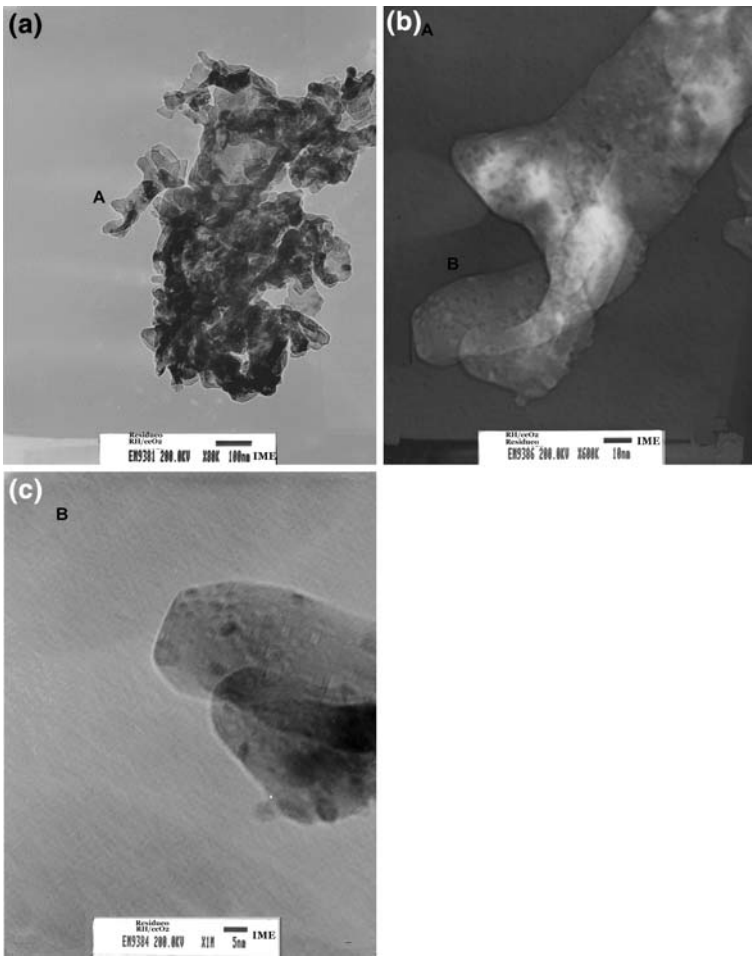

Fig. 15 TEM images (80,000×, 800,000× and 1 Mx, respectively) of Rh/CeO_2 residue

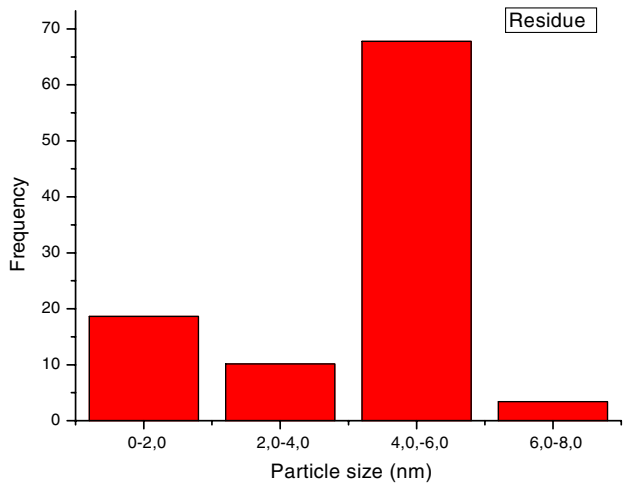

Fig. 16 Particle size distribution histogram of the residue

Acknowledgements We would like to thank Professor Luiz Henrique de Almeida and, especially, chemist Carla Woyames Gabriel at the Microscopy and Microanalysis laboratory of the Metallurgical and Materials Engineering Program at COPPE/UFRJ for their technical support. Daniele Dionisio at the Catalysis Center (NUCAT)/COPPE/UFRJ is also thanked for carrying out the fluorescence analysis. CNPq is also acknowledged for financial support provided for Lídia Oazem de Oliveira da Costa.

References

1. Mattos LV, Noronha FB (2005) J Catal 233:453
2. Hirschenhofer JH, Stauffer DB, Engleman RR, Klett MG (1998) Fuel Cell Handbook, 4th edn
3. Lamy C (2003) In: Proceedings of the XII Brazilian Catalysis Congress, Angra dos Reis, Rio de Janeiro, CD ROM
4. Ramachandran R, Menon RK (1998) Int J Hydrogen Energy 23:593
5. Mattos LV, Noronha FB (2005) J Power Sources 152:50
6. Mattos LV, Noronha FB (2005) J Power Sources 145:10
7. Silva AM, Barandas APMG, Costa LOO, Borges LEP, Mattos LV, Noronha FB, Catalysis Today, in press
8. Chen H, Liu S, Ho J (2006) J Phys Chem B 110:14816–14823
9. Silva AM, Costa LOO, Barandas APMG, Fonseca EV, Mattos LV, Borges LEP, Noronha FB In: Proceedings of the XX Ibero-American Catalysis Symposium, September 2006, Gramado (Rio Grande do Sul, 2006) CD ROM
10. Idriss H (2004) Platinum Metals Rev 48:105
11. Mavrikakis M, Barteau MA (1998) J Mol Catal A 131:135
12. Ruckenstein E, Wang HY (1999) J Catal 187:151
13. Cavallaro S, Mondello N, Freni S (2001) J Power Sources 102:198

14. Cavallaro S, Chiodo V, Vita A, Freni S (2003) J Power Sources 123:10–16
15. Diagne C, Idriss H, Kiennemann A (2002) Catal Commun B 3:563
16. Ruckenstein E, Wang HY (2000) J Catal 190:32
17. Tauster SJ (1978) Acc Chem Res 20:389
18. Vannice MA (1992) Catal Today 12:255
19. Laosiripojana N, Assabumrungat S (2006) Appl Catal B Environ 66:29
20. Passos FB, Aranda DAG, Schmal M (2000) Catal Today 57:283
21. Cesar DV, Pérez CA, Salim VM, Schmall M (1999) Appl Catal A Gen 176:205
22. JCPDS-Joint Committee on Powder Diffraction Standards, International Center of Diffraction Data (1994) Pensiilvania, USA, CD ROM
23. Costa LOO (2007) Catalysts development for hydrogen production for fuel cells from ethanol partial oxidation, Doctoral Thesis, Military Engineering Institute, IME, Rio de Janeiro, Brazil
24. Mendes FMT, Schmal M (1997) Appl Catal A Gen 151:393
25. Bernal S, Calvino JJ, Cauqui MA, Gatica JM, Larese C, Pérez Omil JA, Pintado JM (1999) Catal Today 50:175
26. Graydon WF, Langan MD (1981) J Catal 69:180
27. Jones SG, Mavrikakis M, Barteau MA, Vohs JM (1998) J Am Chem Soc 120:3196
28. Sheng PY, Yee GA, Bowmaker GA, Idriss H (2002) J Cat 208:393
29. Akita T, Tanaka K, Kohyama M, Haruta M (2007) Catal Today 122:233